Eur. Phys. J. A **11**, 237–245 (2001)

THE EUROPEAN PHYSICAL JOURNAL A

Medium effects in the production and $\pi^0\gamma$ decay of ω-mesons in pA collisions in the GeV region

Ye.S. Golubeva[1], L.A. Kondratyuk[2], M. Büscher[3,a], W. Cassing[4], V. Hejny[3], and H. Ströher[3]

[1] Institute of Nuclear Research, 117312 Moscow, Russia
[2] Institute of Theoretical and Experimental Physics, 117259 Moscow, Russia
[3] Forschungszentrum Jülich, Institut für Kernphysik, 52425 Jülich, Germany
[4] Institute for Theoretical Physics, University of Giessen, D-35392 Giessen, Germany

Received: 2 April 2001 / Revised version: 23 May 2001
Communicated by A. Schäfer

Abstract. The ω resonance production and its $\pi^0\gamma$ decay in pA reactions close to threshold is considered within the Intranuclear Cascade (INC) model. The $\pi^0\gamma$ invariant-mass distribution shows two components which correspond to the ω decay "inside" and "outside" the nucleus, respectively. The "inside" component is distorted by medium effects, which introduce a mass shift as well as collisional broadening for the ω-meson and its decaying pion. The relative contribution of the "inside" component is analyzed in detail for different kinematical conditions and nuclear targets. It is demonstrated that a measurement of the correlation in azimuthal angle between the π^0 and γ momenta allows to separate events related to the "inside" ω decay from different sources of background when uncorrelated π^0's and γ's are produced.

PACS. 25.40.Ep Inelastic proton scattering – 25.80.-e Meson- and hyperon-induced reactions – 25.80.Ek Pion inelastic scattering

1 Introduction

The question about the modifications of the vector meson properties in the nuclear medium has received a vivid attention during the last years (cf. refs. [1–12]). Whereas the ρ-meson is expected to practically dissolve already at normal nuclear matter density ρ_0, the ω-meson is expected to survive as a quasi-particle at densities $\leq \rho_0$, *i.e.* in ordinary nuclei. A meson or baryon resonance produced in a pion- or proton-induced reaction on nuclei can decay "outside" or "inside" the target nucleus. Correspondingly, the invariant-mass distribution of the decay products for each resonance contains two components [8,12]. The first component is described by a Breit-Wigner formula with vacuum properties of the resonance mass M_0 and width Γ_0. The second component is strongly distorted by the nuclear medium due to a collisional broadening $\delta\Gamma$ and a possible mass shift δM, where in first approximation $\delta\Gamma$ and δM are proportional to the nuclear density. In principle, medium modifications of ω-mesons can be detected directly by measuring the dilepton invariant-mass spectra in hA and AA collisions (see, *e.g.* refs. [12,13] and references therein). The advantages of this method are related to the fact that the dilepton mass spectra are almost undistorted by the final-state interactions. However, the ω signal in the dilepton mode is rather weak ($\mathrm{BR}(\omega \to e^+e^-) \simeq 7.1 \times 10^{-5}$) and is always accompanied by a comparatively large background from ρ^0 decays. From this point of view it is useful to consider also the $\omega \to \pi^0\gamma$ decay which has a branching ratio of about 3 orders of magnitude higher (see refs. [14,15]). Furthermore, the competing $\rho^0 \to \pi^0\gamma$ channel has a branching ratio of only $7.9 \pm 2.0 \times 10^{-4}$ which is about a factor 10^2 smaller than the $\omega \to \pi^0\gamma$ decay with a branching ratio of $8.5 \pm 0.5\%$. As it was shown in ref. [15] the effect of the ω mass shift in the $\pi^0\gamma$ invariant-mass distribution can be identified on top of the background which is dominantly related to $\pi^0 N$ rescattering events.

In the present paper we discuss in more detail the in-medium ω decay to an off-shell π^0 and a photon and investigate additional criteria to separate the $\omega \to \pi^0\gamma$ signal in pA collisions at GeV energies from different sources of background such as $\pi^0\pi^0$ or $\pi^0\eta$ when one photon from the meson decays is not detected or misidentified.

The paper is organized as follows: In sect. 2 we will briefly discuss the propagation of a resonance in the nuclear medium, its decay to an off-shell pion and a photon and describe the Intranuclear Cascade (INC) model that is used in the simulation of events for the reaction $pA \to \omega(\pi^0\gamma)X$. In sect. 3 we present the results of our calculations and summarize our work in sect. 4.

[a] e-mail: m.buescher@fz-juelich.de

2 Theoretical framework

2.1 Propagation of a resonance in the nuclear medium

We here consider the production of ω resonances in pA collisions not far above the threshold. Due to the kinematics of the production process, the resonance will be quite fast in the laboratory frame (with the target almost at rest) and its propagation through the nucleus can be described within the framework of the eikonal approximation. The corresponding Green function, which describes the propagation of the resonance from the point $\vec{r} = (\vec{b}, z)$ (where it is produced) to the point $\vec{r}\,' = (\vec{b}\,', z')$ (where it decays or rescatters incoherently) can be written as [8,12]

$$G_p(\vec{b}\,', z'; \vec{b}, z) = \frac{1}{2ip} \exp\left\{ i \int_z^{z'} \left[p + \frac{1}{2p}(\Delta + 4\pi f(0)\rho_A(\vec{b}, \zeta)) \right] \mathrm{d}\zeta \right\} \times \delta(\vec{b} - \vec{b}\,')\theta(z' - z), \quad (1)$$

where the z-axis is directed along the resonance momentum $\vec{p}$, $\vec{b}$ is the impact parameter and

$$\Delta = P^2 - M_{\mathrm{R}}^2 + iM_{\mathrm{R}}\Gamma_{\mathrm{R}} \quad (2)$$

is the inverse resonance propagator, while M_{R} and Γ_{R} are the resonance mass and width in the vacuum. The four-momentum P in (2) can be defined through the four-momenta of the resonance decay products,

$$P = p^*(\pi^0) + p(\gamma), \quad (3)$$

where $p^*(\pi^0)$ is the pion 4-momentum in the medium (cf. sect. 2.2). Equation (1) is written in the low-density approximation with the optical potential defined as (see, *e.g.* ref. [16])

$$U(\vec{r}) = -4\pi f(0)\rho_A(\vec{r}), \quad (4)$$

where $f(0)$ is the forward ωN scattering amplitude and $\rho_A(\vec{r})$ is the nuclear density.

The corresponding amplitude, which describes the production of the resonance in the point $\vec{r} = (\vec{b}, z)$ inside the nucleus and its decay in the point $\vec{r}\,' = (\vec{b}\,', z')$, can be written as

$$M(\vec{P}, P^2; \vec{b}, z) = B f_{pN_j \to \omega X_i} \int \mathrm{d}^2\vec{b}\,' \mathrm{d}z' \{\exp(-i\vec{p}\,\vec{r}\,')G_p(\vec{r}\,' - \vec{r}\,)\exp(i\vec{p}\,\vec{r}\,')\} \times f_{\omega \to \pi^0\gamma}. \quad (5)$$

Here $f_{pN_j \to \omega X_i}$ is the production amplitude; $X_i = NN, \pi NN, \Delta N, ...$; $f_{\omega \to \pi^0\gamma}$ is the decay amplitude and B is a normalization factor which takes into account the attenuation of the initial proton flux due to the screening from other nucleons.

Since we consider energies not far above threshold for ω production, the ω can be produced in the first hard proton-nucleon collision or through the two-step mechanism with an intermediate production of a pion [17,18]: $pN_j \to \pi pN, \pi N_k \to \omega N$. The contribution of the two-step scattering mechanism has to be added to the direct mechanism described by eq. (5). In the latter case, the production amplitude is obtained by replacing $f_{pN_j \to \omega X_i}$ in (5) by $f_{\pi N_k \to \omega X_i}$ and G_p by the pion propagator G_π. In addition an integration over all pion production points has to be performed.

If the resonance decays outside the nucleus of radius R, the amplitude for $\pi^0\gamma$ production —in case of the primary production channel— can be written as

$$M_j^i(\vec{P}, P^2; \vec{b}, z) = Bf(pN_j \to \omega X_i)\{A_{\mathrm{in}}(\vec{P}, P^2; \vec{b}, z) + A_{\mathrm{out}}(\vec{P}, P^2; \vec{b}, z)\} \times f_{\omega \to \pi^0\gamma}\,, \quad (6)$$

where the contributions from the resonance decays "inside" and "outside" the nucleus can be expressed as

$$A_{\mathrm{in}}(\vec{P}, P^2; \vec{b}, z) = \frac{1 - \exp[i(\Delta^*/2k)(z_s - z)]}{\Delta^*}\,, \quad (7)$$

and

$$A_{\mathrm{out}} = \frac{\exp[i(\Delta^*/2k)(z_s - z)]}{\Delta}\,, \quad (8)$$

with $z_s = \sqrt{R^2 - \vec{b}^2}$ and

$$\Delta^* = \Delta + 4\pi f(0)\rho_0 = P^2 - M_{\mathrm{R}}^{*2} + iM_{\mathrm{R}}^*\Gamma_{\mathrm{R}}^*. \quad (9)$$

Equation (9) describes the resonance propagator $(\Delta^*)^{-1}$ in the nuclear medium with distorted values of the resonance mass ($M_{\mathrm{R}}*$) and width (Γ_{R}^*) defined by

$$M_{\mathrm{R}}^{*2} = M_{\mathrm{R}}^2 - 4\pi \mathrm{Re} f(0)\rho_A\,, \quad (10)$$

$$M_{\mathrm{R}}^*\Gamma_{\mathrm{R}}^* = M_{\mathrm{R}}\Gamma_{\mathrm{R}} + 4\pi \mathrm{Im} f(0)\rho_A\,. \quad (11)$$

When the resonance decays "inside" the nucleus the amplitude (6) contains only the "inside" component A_{in} defined by (7). Evidently, the $\pi^0\gamma$ invariant-mass spectrum is given by the following expression:

$$\frac{\mathrm{d}\sigma}{\mathrm{d}M} = \sum_{i,j} \int \mathrm{d}^2b\mathrm{d}z\ \rho(\vec{b}, z)\ |M_j^i(\vec{P}, \vec{P}^{\,2}, \vec{b}, z)|^2\,, \quad (12)$$

where the sum is taken over all nucleons in the target and all production channels, respectively.

2.2 ω decay to off-shell pions

Since not only the ω-meson, but also the decay pion changes its spectral function in the medium, the in-medium ω Dalitz decay has to be discussed explicitly. Now let the in-medium ω mass be M and the decay pion have a mass m_π^* that might be selected by Monte Carlo according to its in-medium spectral function with width Γ_π^* and

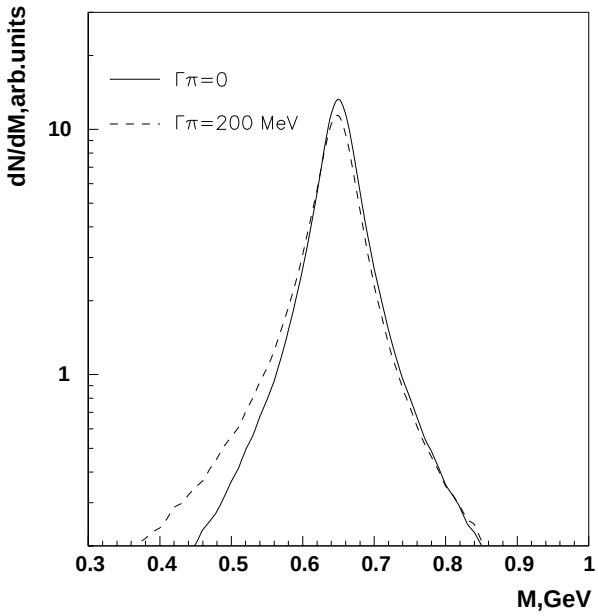

Fig. 1. Invariant-mass distribution of in-medium ω decays to $\pi^0\gamma$ as reconstructed within on-shell pion dynamics (solid line) in comparison to off-shell pion dynamics (dashed line) for a pion spectral function with a collisional width of 200 MeV.

mass shift δm_π. Energy and momentum conservation —in the rest frame of the ω-meson— then implies

$$M^2 = (E_\pi^* + E_\gamma)^2 = (\sqrt{p_\pi^{*2} + m_\pi^{*2}} + E_\gamma)^2, \qquad (13)$$

with $E_\gamma = |p_\pi^*|$ denoting the photon energy which in magnitude equals the momentum of the decay pion. Whereas the photon propagates to the vacuum without distortion, the in-medium pion changes its momentum and spectral function during the propagation to the vacuum according to quantum off-shell propagation [19–21]. In the particular case, where the pion self-energy Σ_π has no explicit time dependence ($\partial_t \Sigma_\pi = 0$) and is only a function of momentum and density, which holds well for the case of $p+A$ reactions, the energy of the pion $E_\pi^* = E_\pi$ is a constant of motion (cf. eq. (20) in ref. [20]). Thus, the off-shell mass and momentum balance out during the propagation as shown graphically in ref. [20] in figs. 1 and 2 for a related problem. The magnitude of the pion momentum in-vacuum —if not scattered explicitly or being absorped— then is simply given by

$$p_\pi^{\rm v} = \sqrt{p_\pi^{*2} + m_\pi^{*2} - m_0^2}\,, \qquad (14)$$

where m_0 denotes the vacuum pion mass and p_π^* the pion momentum in the ω decay in-medium. The invariant mass (squared) of the pion and photon in the vacuum then is given by

$$M_r^2 = (E_\pi + E_\gamma)^2 - (p_\pi^{\rm v} - E_\gamma)^2 = M^2 - (p_\pi^{\rm v} - E_\gamma)^2\,. \qquad (15)$$

The pion propagation thus leads to a slight downward shift of the invariant mass in-vacuum relative to its original in-medium value. We note, that the above considerations apply well for heavy nuclei where the corrections in energy due to the recoil momentum of the nucleus ($|p_\pi^{\rm v} - E_\gamma|$) can be discarded.

For an actual quantification of this effect one has to specify the pion spectral function, *e.g.* at nuclear matter density (assuming a linear dependence on density ρ for simplicity). The pions, that originate from the ω decay in $p+A$ reactions, have typical momenta $\geq$ 300 MeV such that their interaction cross-section with nucleons is in the order of 30–35 mb, while their velocity β_π relative to the target is close to 1. Consequently, the collisional broadening can be estimated as

$$\delta\Gamma_\pi \approx \beta_\pi \sigma_{\pi N} \rho_0 \approx 100\text{–}120 \text{ MeV}, \qquad (16)$$

which is still quite substantial. For the ω in-medium spectral function we assume a Breight-Wigner of width $\Gamma_{\rm tot} = 50$ MeV and pole mass of 0.65 GeV (cf. solid line in fig. 1). Now for each invariant mass M the decay of the ω to a photon and an in-medium pion can be evaluated and the pion momentum $p_\pi^{\rm v}$ according to (14). To obtain some upper limit for the pion off-shell effects we take $\delta\Gamma_\pi = 200$ MeV. The reconstructed invariant-mass distribution in (15) is shown in fig. 1 by the dashed line, which is close to the original ω spectral function (solid line) and indicates that such corrections can be safely neglected in view of presently achievable experimental mass resolutions. Furthermore, the effects are most pronounced for very low invariant masses M where, however, the spectrum is strongly distorted by π^0 rescattering (see below). Thus, we continue our calculations with on-shell spectral functions for the pions without substantial loss in accuracy. For the general case of off-shell dynamics in transport or cascade calculations we refer the reader to refs. [19–21].

2.3 The Intranuclear Cascade model and interaction parameters

The yields of ω-mesons are calculated within the framework of the Intranuclear Cascade model (INC) developed in ref. [18,22], which was also used in ref. [12] for the analysis of medium effects for ω's produced in pion-nucleus reactions with respect to their dilepton decay. In the INC the linearized kinetic equation for the many-body distribution function is solved numerically by assuming that during the evolution of the cascade, the properties of the target nucleus remain unchanged. Within the INC approach the target nucleus is regarded as a mixture of degenerate neutron and proton Fermi gases in a spherical potential well with a diffuse surface. The momentum distribution of the nucleons is treated in the local density approximation for a Fermi gas.

The following inputs were used for the elementary cross-sections (see also refs. [18,22]: i) For the cross-section of the reaction $pN \to \omega pN$ we use parametrization from ref. [17]. ii) For the process $\pi^- p \to \omega n$ we use a parametrization of the experimental data from refs. [18,23]:

$$\sigma(\pi^- p \to \omega n) = C \frac{P_{\pi N} - P_\omega^0}{P_{\pi N}^\alpha - d}, \qquad (17)$$

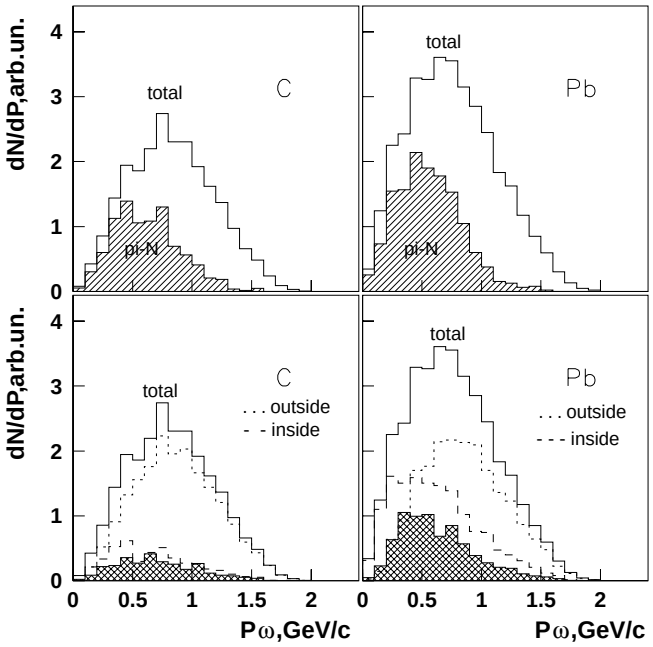

Fig. 2. Momentum distributions of ω-mesons in the reactions $p + {}^{12}$C (l.h.s.) and $p + {}^{208}$Pb (r.h.s.) at $T_p = 2.4$ GeV (solid histograms). The contributions from the two-step ω production mechanism is shown by the hatched areas in the upper parts. The dotted and dashed histograms in the lower parts correspond to ω decays "outside" and "inside" the nucleus, respectively. The hatched areas in the lower figures describe the contribution from the "inside" component with surviving pions, *i.e.* for pions from the ω decay that propagate to the vacuum, however, may rescatter elastically.

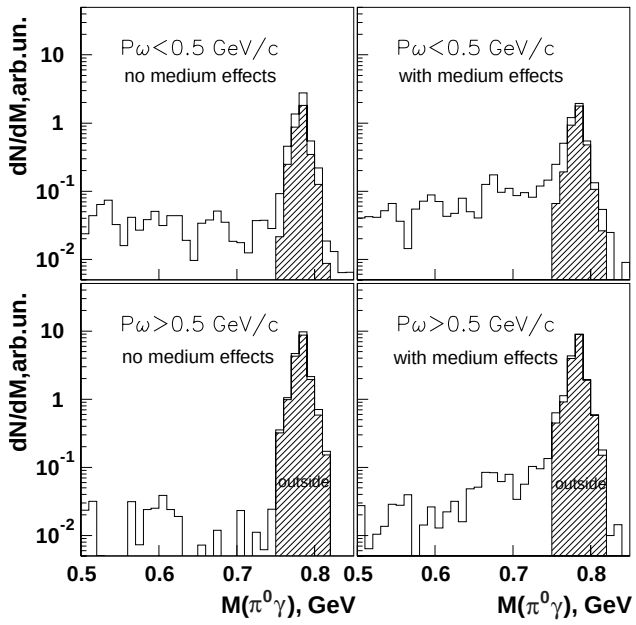

Fig. 3. The $\pi^0\gamma$ invariant-mass spectra for p+Pb collisions at $T_p = 2.4$ GeV. The upper and lower histograms are calculated for "slow" ($p_\omega \leq 0.5$ GeV/c) and "fast" ($p_\omega \geq 0.5$ GeV/c) ω-mesons, respectively. The right (left) figures show the distributions with (without) medium effects. The hatched areas correspond to ω decays outside the nucleus.

where $P_{\pi N}$ is the relative momentum (in GeV) of the pion-nucleon pair while $P^0_\omega = 1.095$ GeV is the threshold value. The parameters $C = 13.76$ mb GeV/$c^{\alpha-1}$, $\alpha = 3.33$ and $d = 1.07$ GeV$^\alpha$ describe satisfactorily the data on the energy-dependent cross-section $\pi^- p \to \omega n$ in the near-threshold energy region. iii) For the ωN elastic and total cross-sections we use the same parametrization as in refs. [12,18]. The angular distributions for the particles produced in the elementary reactions are considered to be isotropic in the corresponding c.m.s. since we operate close to threshold energies.

The propagation of vector mesons in the nuclear medium is described in the same manner as in our previous works [12]. A collisional broadening of the resonance in the nuclear medium is introduced according to eq. (11) where $\mathrm{Im}f(0)$ has been expressed through $\sigma_{\mathrm{tot}}(\omega N)$ using the optical theorem. The ω mass shift is modeled according to Hatsuda and Lee [5] as

$$M^*_{\mathrm{R}} = M_{\mathrm{R}} + \delta M_{\mathrm{R}} = M_{\mathrm{R}} \left(1 - \alpha \frac{\rho_A(r)}{\rho_0}\right), \qquad (18)$$

where $\rho_A(r)$ is the nuclear density at the resonance decay point, $\rho_0 = 0.16\,\mathrm{fm}^{-3}$, and $\alpha = 0.18$.

The decay of the ω to $\pi^0\gamma$ with its actual spectral shape is performed as in ref. [12]: when the resonance decays inside the nucleus, its mass is generated according to a Breit-Wigner distribution with average mass M^*_{R} (18) and $\Gamma^*_{\mathrm{R}} = \Gamma_{\mathrm{R}} + \delta\Gamma_{\mathrm{R}}$ (see (11)), where the collisional broadening and the mass shift are calculated according to the local nuclear density. Its decay to $\pi^0\gamma$ is recorded as a function of the corresponding invariant-mass bin and the local nucleon density ρ_A. If the resonance leaves the nucleus, its spectral function automatically coincides with the free distribution because δM_{R} and $\delta\Gamma_{\mathrm{R}}$ are zero in this case. Secondary interactions of π^0 from ω decay are taken into account using realistic $\pi^0 N$ elastic, inelastic and charge exchange cross-sections.

3 Production and $\pi^0\gamma$ decay of ω-mesons

3.1 General aspects

We continue with the actual numerical results of our calculations and first have a look at the ω momentum distributions in the laboratory for p+A collisions at $T_p = 2.4$ GeV. The solid histograms in fig. 2 show the calculated momentum distributions of ω-mesons in the reactions $p + {}^{12}$C (left figures) and $p + {}^{208}$Pb (right figures). Hatched areas in the upper part of the figure describe the contributions from the two-step ω production mechanism with an intermediate pion, which have a maximum at slightly lower momenta than the total spectrum (solid histograms) for both targets due to the different kinematics. The dotted and dashed histograms in the lower part of fig. 2 correspond to ω decays "outside" ($\rho \leq 0.03\ \rho_0$) and "inside"

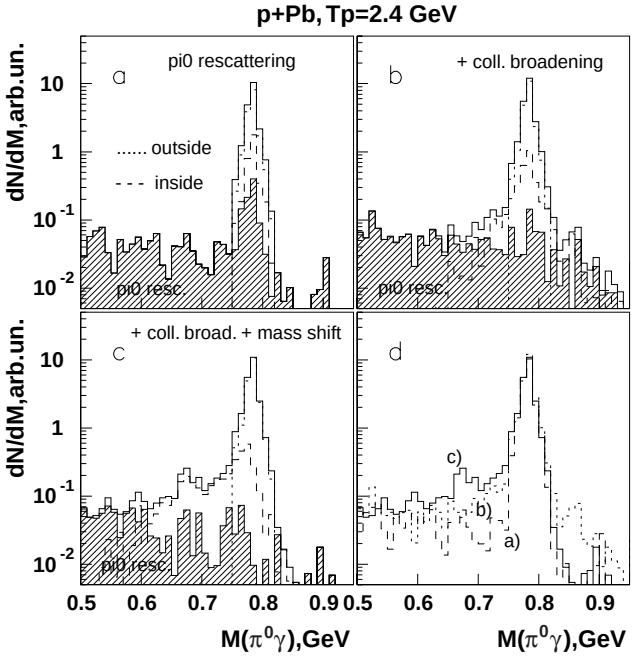

Fig. 4. The $\pi^0\gamma$ invariant-mass distributions in p + Pb collisions at T_p = 2.4 GeV for different scenarios: a) no ω in-medium effects are taken into account and all the distorsion of the $M(\pi^0\gamma)$ spectrum from the ω decay is caused by π^0 rescattering; b) the collisional broadening $\delta\Gamma$ is included for the ω spectral function but no mass shift; c) both in-medium effects $\delta\Gamma$ and δM are taken into account; d) the dashed, dotted and solid curves correspond to the solid curves in a), b) and c), respectively. The hatched areas in a)-c) describe events with rescattered pions. The dotted histograms in a)-c) show events with ω's decaying outside, while the dashed histograms correspond to ω's decaying inside the nucleus with their rescattering switched off.

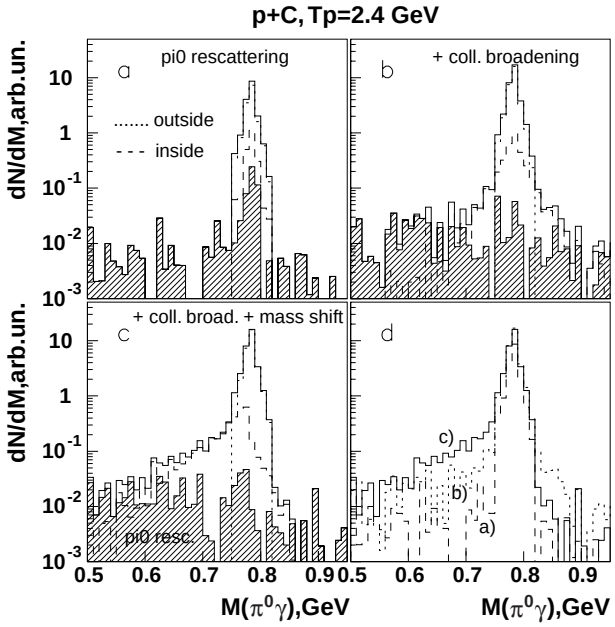

Fig. 5. The $\pi^0\gamma$ invariant-mass distributions in p+C collisions at T_p = 2.4 GeV, respectively. The meaning of the histograms is the same as in fig. 4.

($\rho \geq 0.03\ \rho_0$) a nucleus, respectively. It is clearly seen that in case of the ^{12}C target most of the ω-mesons decay in the vacuum (dotted histogram) while in case of the Pb target both components (integrated over momentum) become roughly comparable. By performing cuts on the ω momentum p_ω one can vary systematically the fraction of "inside" (dashed histogram) to "outside" decays (dotted histogram). Furthermore, the hatched areas in the lower part of fig. 2 represent the events from the "inside" component with surviving neutral pions, *i.e.* with π^0's which propagate to the vacuum. Note, that this contribution includes also pions that rescatter elastically. The latter component (of surviving neutral pions) is dominant for the "inside" decay in case of the ^{12}C target, but reduces to roughly 60% for the Pb target. Nevertheless, there is still a large fraction of π^0's that escape without rescattering, since for ω-mesons with momenta around 0.5 GeV/c the decaying pions also have large momenta with respect to the target (at rest in the laboratory) such that their interaction cross-section with nucleons is only about 30–35 mb.

The upper and lower histograms in fig. 3 show the $\pi^0\gamma$ invariant-mass spectra from p + Pb collisions at 2.4 GeV for slow ($p_\omega \leq 0.5$ GeV/c) and fast ($p_\omega \geq 0.5$ GeV/c) ω-mesons, respectively. The right (left) figures demonstrate the distributions with (without) medium effects for the ω-mesons taken into account whereas the hatched areas correspond to ω decays outside the nucleus. As seen from a comparison of the left and right figures, the events with invariant mass $M(\pi^0\gamma) \leq 0.75$ GeV come up not only due to a collisional broadening and/or mass shift of ω-mesons but also due to π^0 rescattering. Especially, for "slow" ω's this π^0 rescattering contribution is more pronounced since in this case the cross-section for π^0 rescattering is quite large such that the interesting signal from the in-medium ω decay is masked substantially.

The question now arises to what extent one might possibly disentangle in-medium effects due to collisional broadening and/or ω-meson mass shifts, respectively. To this aim we have performed calculations for a Pb target (fig. 4) and a ^{12}C target (fig. 5) at 2.4 GeV for different assumptions on the in-medium properties of the ω-meson. In both figures we present again the $\pi^0\gamma$ invariant-mass distributions, however, without performing cuts on the ω momentum. Figures 4a) and 5a) show the invariant-mass distributions when ω medium effects are discarded and all the distorsion of the $M(\pi^0\gamma)$ spectrum from ω decay is due to π^0 rescattering. Parts b) of figs. 4 and 5 demonstrate the $\pi^0\gamma$ invariant-mass spectrum when only the collisional broadening $\delta\Gamma$ is taken into account while in parts c) both in-medium effects, *i.e.* $\delta\Gamma$ and δM are taken into account. The hatched areas in parts a)-c) show the events with rescattered pions, the dotted histograms in a)-c) describe the events with ω's decaying outside, while the dashed histograms correspond to ω's decaying inside the nucleus with π^0 rescattering switched off, such that the ω spectral function at the decay becomes visible explicitly.

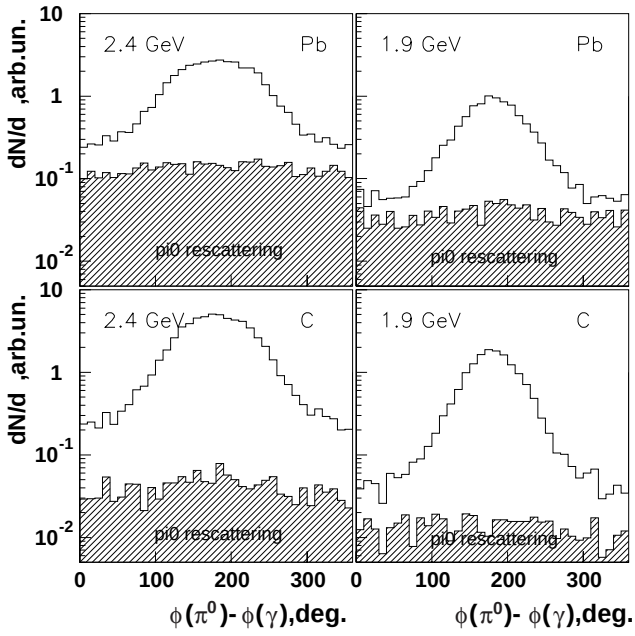

Fig. 6. The distributions in azimuthal angle between two planes $\phi = \phi_{\pi^0} - \phi_\gamma$, where one plane is formed by the initial proton momentum and the final π^0 momentum ($\mathbf{p}_0 \wedge \mathbf{p}_{\pi^0}$) and the second one is formed by the initial proton momentum and the γ momentum ($\mathbf{p}_0 \wedge \mathbf{p}_\gamma$). The solid histograms describe the distributions $\mathrm{d}N/\mathrm{d}\phi$ from $p + \mathrm{Pb}$ (upper part) and $p + \mathrm{C}$ collisions (lower part) at $T_p = 2.4$ GeV (left) and 1.9 GeV (right) for ω's decaying inside. The hatched histograms show the events with rescattered pions. The solid histograms have distinctive maxima at $\phi = 180°$ which correspond to correlated π^0 and γ pairs from the ω decay.

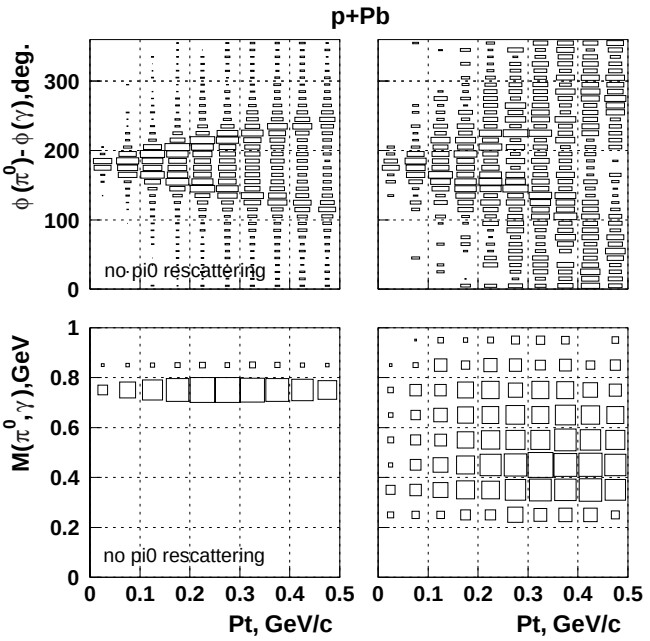

Fig. 7. Two dimensional plots for the distribution in the azimuthal angle ϕ *versus* the ω transverse momentum P_t (upper part) and the invariant mass $M(\pi^0, \gamma)$ *versus* P_t (lower part) for $p + \mathrm{Pb}$ at $T_p = 2.4$ GeV. The left plots describe the events, where the rescattering of pions is switched off, while in the right plots only events with rescattered pions are selected.

For an actual comparison of the different scenarios the parts d) in figs. 4 and 5 show the total spectra from a)-c) again: the dashed histograms correspond to the calculations without in-medium effects (a), the dotted histograms to the spectra including collisional broadening $\delta\Gamma \neq 0$ but without a mass shift $\delta M = 0$ (b), while the solid histograms show the result with collisional broadening $\delta\Gamma \neq 0$ and the mass shift $\delta M \neq 0$ (c). In the region $M(\pi^0\gamma) = 0.65$–0.75 GeV there is a substantial enhancement in the spectrum due to medium effects (solid histograms) relative to the vacuum ω decays (dashed histogram) even when including π^0 rescattering. This finding is in agreement with the results of previous calculations on the ω properties from pion- and proton-induced reactions on nuclei, that have investigated the ω dilepton or $\pi^0\gamma$ decay [12,14,15], respectively.

3.2 Background reduction

Experiments on ω production in nuclei might be carried out at the proton accelerator COSY-Jülich using a photon detector to look for the 3γ invariant-mass distribution and selecting 2γ's in the invariant-mass region of the π^0, that stem from the decay of the neutral pion. However, in the mass region $M(\pi^0\gamma) = 0.65$–0.75 GeV there might be essential "background" with 3 (non-resonant) γ's in the final state or from four photon final states (*e.g.*, the decay products from $2\pi^0$, $\eta\pi^0$ etc.) when one photon is not identified due to the finite geometrical acceptance of the detector. In the following, a method is outlined which will help to identify events where the 3γ's in the final state are, in fact, produced via ω-mesons.

It is possible to exploit, for example, kinematical conditions. When an ω-meson is produced not far above threshold it will have comparatively small transverse momentum P_t in the lab. system. In this case we can expect that the π^0 and γ from the ω decay will be strongly correlated in their transverse momenta, while $\pi^0\gamma$ events from the background will not show such a correlation. In order to investigate this momentum correlation in the case of ω decays inside the nucleus we present in fig. 6 the distributions in the azimuthal angle between two planes $\phi = \phi_{\pi^0} - \phi_\gamma$, where one plane is formed by the initial proton momentum and the final π^0 momentum ($\mathbf{p}_0 \wedge \mathbf{p}_{\pi^0}$) and the second one is formed by the initial proton momentum and the γ momentum ($\mathbf{p}_0 \wedge \mathbf{p}_\gamma$). The solid histograms in fig. 6 describe the distributions $\mathrm{d}N/\mathrm{d}\phi$ from $p + \mathrm{Pb}$ (upper part) and $p + {}^{12}\mathrm{C}$ collisions (lower part) at $T_p = 2.4$ GeV (left) and 1.9 GeV (right) for "inside" ω decays. The hatched histograms, which describe events with rescattered pions, are essentially flat and do not show any correlation between the π^0 and γ. At the same time the solid histograms have distinctive maxima at $\phi = 180°$ which correspond to correlated π^0 and γ events from the ω decay. The width of the distribution in $\mathrm{d}N/\mathrm{d}\phi$ depends on the ω-meson transverse

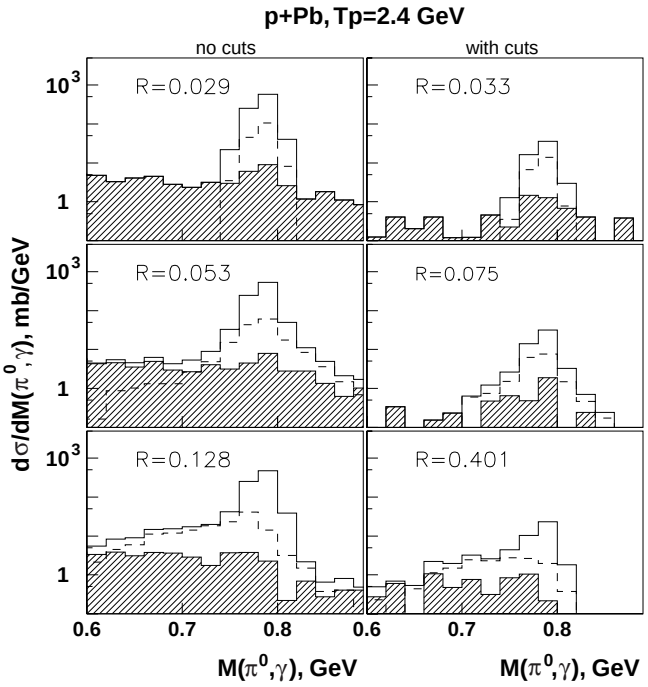

Fig. 8. The ratio R (20) for $p+\mathrm{Pb}$ collisions calculated without cuts (l.h.s.) and with cuts (r.h.s.) on the total and transverse momentum of the $\pi^0\gamma$ system $P_{\rm tot} \leq 0.5$ GeV/c, $P_{\rm t} \leq 0.2$ GeV/c and the azimuthal angle $\phi = \phi_{\pi^0} - \phi_\gamma = 180 \pm 30^\circ$.

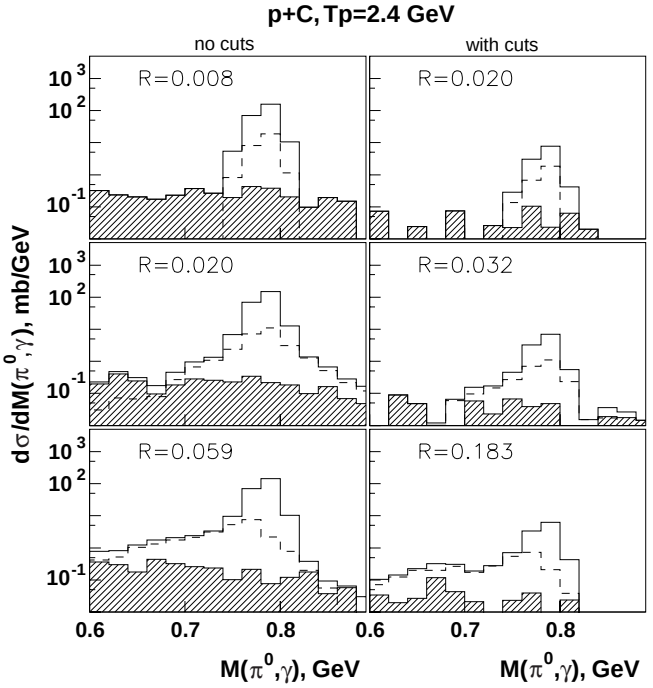

Fig. 9. The same distributions as in fig. 8 for $p+\mathrm{C}$ collisions.

momentum $P_{\rm t}$. Therefore it becomes more narrow with decreasing initial energy T_p; very close to the threshold it will depend essentially on the Fermi motion of the target nucleons and effects from ω rescattering. These rescattering effects are smaller for ^{12}C than for Pb (compare upper and lower solid histograms in fig. 6). Nevertheless, the azimuthal correlation remains quite pronounced also for Pb even at $T_p = 2.4$ GeV.

In fig. 7 we present two dimensional plots for the distribution in the azimuthal angle ϕ *versus* the ω transverse momentum $P_{\rm t}$ (upper part) and in the invariant mass $M(\pi^0,\gamma)$ *versus* $P_{\rm t}$ (lower part) for $p+\mathrm{Pb}$ at $T_p = 2.4$ GeV. The l.h.s. describes events, where the rescattering of pions is switched off, while in the r.h.s. only events with rescattered pions are selected. By comparing the left and right distributions in fig. 7 we conclude that the relative contribution of the background from π^0 rescattering can be essentially suppressed choosing the cut $P_{\rm t} \leq 0.2$ GeV/c. This is demonstrated in more detail in fig. 8 (for $p+\mathrm{Pb}$) and fig. 9 (for $p+\mathrm{C}$) at $T_p = 2.4$ GeV, where we present the ratio

$$R = \frac{N(M(\pi^0,\gamma) = 0.6\text{–}0.75 \text{ GeV})}{N(M(\pi^0,\gamma) \geq 0.75 \text{ GeV})} \qquad (19)$$

calculated without cuts for the left histograms and with cuts on the total and transverse momentum of the $\pi^0\gamma$ system $P_{\rm tot} \leq 0.5$ GeV/c, $P_{\rm t} \leq 0.2$ GeV/c and the azimuthal angle $\phi = \phi_{\pi^0} - \phi_\gamma = 180 \pm 30^\circ$ for the right histograms. Without cuts the ratio R for Pb (C) changes from 0.029 (0.008) —when medium effects are absent (upper left histograms) —to 0.053 (0.020) when only collisional broadening is taken into account (middle left histograms) and reaches 0.128 (0.059) when both medium effects —collisional broadening and mass shift— are included (lower left histograms). The calculations with cuts give the ratio $R = 0.033$ (0.020) without medium effects (upper right histograms), 0.075 (0.032) with $\delta\Gamma \neq 0$ but without mass shift (middle right histograms) and 0.401 (0.183) with collisional broadening $\delta\Gamma \neq 0$ and mass shift $\delta M \neq 0$ (lower right), respectively. Therefore, using cuts on the total and transverse momentum of the $\pi^0\gamma$ system ($P_{\rm tot} \leq 0.5$ GeV/c, $P_{\rm t} \leq 0.2$ GeV/c) and the azimuthal angle $\phi = \phi_{\pi^0} - \phi_\gamma = 180 \pm 30^\circ$ it is possible to increase essentially the relative contribution of medium effects and to suppress the background from π^0 rescattering or related uncorrelated sources. We point out again, that the cut in the azimuthal angle ϕ is important to suppress different sources of background which contain uncorrelated $\pi^0\gamma$ pairs.

The energy dependence of the ω production cross-section on Pb (upper figure) and C (lower figure) multiplied by the branching $\mathrm{BR}(\pi^0\gamma)$ is shown in fig. 10. The dotted and dash-dotted curves correspond to ω decays "outside" and "inside" the nucleus, respectively, where the "inside" component corresponds to events with a neutral pion (and photon) in the final state. It thus does not include π^0 absorption or pion charge exchange reactions. The solid lines describe the total ω yield in the final $\pi^0\gamma$ channel, while the dashed lines are calculated for the events with pion elastic rescattering from "inside" ω decays. The total cross-section increases from 20 (3) μb at $T_p = 1.7$ to about 300 (40) μb at 2.6 GeV for a Pb (^{12}C) target, whereas the ratio of the "inside" to "outside"

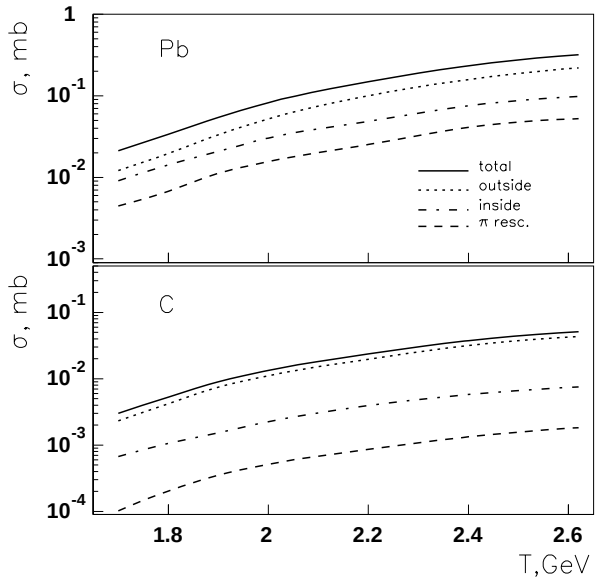

Fig. 10. The energy dependence of the ω production cross-section on Pb (upper part) and ^{12}C (lower part) multiplied by the branching BR($\pi^0\gamma$). The dotted and dash-dotted lines correspond to ω decays "outside" and "inside" the nucleus, respectively, where the "inside" component corresponds to events with a neutral pion (and photon) in the final state. It thus does not include π^0 absorption or pion charge exchange reactions. The solid curve describes the total ω yield in the final $\pi^0\gamma$ channel, while the dashed line reflects events with pion elastic rescattering from the "inside" component of the ω decay.

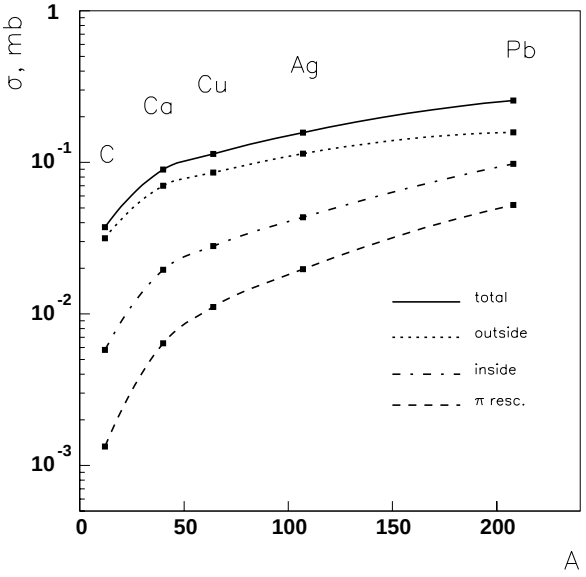

Fig. 11. The target A-dependence of the ω production cross-section in the $\pi^0\gamma$ channel at $T_p = 2.4$ GeV. The notation of the lines is the same as in fig. 10.

component of the ω decay slightly decreases with bombarding energy due to kinematics. Since this ratio as well as the relative amount of π^0 elastic rescattering changes only smoothly with bombarding energy, experiments at the highest energy of $T_p = 2.6$ GeV are clearly favored.

The target mass (A)-dependence of the ω production cross-section in the final $\pi^0\gamma$ channel at 2.4 GeV is presented in fig. 11, where the notation of the curves is the same as in fig. 10. Here the ratio of "inside" (dash-dotted) to "outside" (dotted) ω decays increases substantially with mass number A, while the relative π^0 rescattering increases with A only moderately. This effect correlates with the average propagation time of the ω-meson in the nucleus.

It is important to note that the actual mass shift of the ω-meson at finite density is not known. In eq. (18) we have used a coefficient $\alpha = 0.18$ as suggested by QCD sum rules [5] for ω-mesons at rest in the nucleus. However, the ω self-energy might well be a function of the momentum as suggested by the studies in refs. [24–27] in case of the ρ-meson. Therefore, the actual mass shift seen in pA reactions might be different; however, when gating on different momentum intervals for the ω-mesons in the laborarory system this information might be determined experimentally, too.

One of the most important source of three photon background is related to the reactions $pp \to p\Delta^+(p\gamma)\pi_0(2\gamma)$ and $pN \to p\Delta^0(n\gamma)\pi_0(2\gamma)$. Taking into account that $\sigma(NN \to N\Delta\pi)$ can be about 1 mb and the branching BR($\Delta \to N\gamma \simeq 5 \times 10^{-3}$) we find that $\sigma_{\rm BG} \simeq 5$ μb per nucleon. At the same time the cross-section σ_0 for the $\pi^0\gamma$ yield from the ω decays inside the nucleus can be written as

$$\sigma_0 = \sigma(pN \to pN\omega) \cdot {\rm BR}(\omega \to \pi^0\gamma) \cdot P({\rm inside})\,, \quad (20)$$

where $\sigma(pN \to pN\omega) \simeq$ 200–300 μb (cf. [28]), BR($\omega \to \pi^0\gamma = 0.085$ while the probability $P_{\rm Pb}$(inside) for the ω to decay inside the Pb nucleus is $\simeq 0.4$ (cf. fig. 2). As a result we have for a Pb target $\sigma_0 \approx$ 7–10 μb per nucleon. This implies that the background is roughly of the same order than the signal from ω production with subsequent decay in the nucleus. However, the non-resonant background has broader angular and 3γ invariant-mass distributions. Thus the analysis procedures outlined above can also be applied for events outside the ω peak and in such a way —although not explicitly shown here— it should be possible to subtract the non-resonant events from "real" ω events which decay in the nucleus.

Another source of background stems from the $\rho^0 \to \pi^0\gamma$ decay, which has similar kinematics than the $\omega \to \pi^0\gamma$ decay and cannot be rejected by the kinematical cuts described above. However, this background is distributed over a wide range of invariant masses since the ρ^0-mesons, that dominantly decay inside the nucleus, have a total width of ~ 250 MeV at normal nuclear matter density [27]. Furthermore, the production cross-section of ρ^0-mesons is the same as for ω-mesons within a factor of 2 [11], but their branching ratio to the $\pi^0\gamma$ channel is lower by about a factor of 10^2 relative to the ω's as noted in the introduction. Since the "in-medium" ω decay fraction is larger than 10% and their "in-medium" width is smaller than the "in-medium" width of the ρ^0's by a factor ~ 5, the contribution of the ρ^0 decays in the differential invariant-mass

spectra is less than 2% of the "in-medium" ω signal. Thus, this competing $\pi^0\gamma$ decay of the ρ^0-meson can clearly be neglected.

4 Summary

In this work we have analyzed the possibility to detect in-medium effects for the ω-meson in the reaction $pA \to \omega(\pi^0\gamma)X$ by detecting 3 photons in the final channel where 2 photons add up in the invariant mass to the π^0 mass. As already shown in ref. [15], the rescattering of pions will not spoil completely the in-medium effect related to the ω-mass shift. Furthermore, we have demonstrated here that the in-medium ω decay to off-shell pions (and γ) does not modify the reconstructed invariant-mass distribution very much relative to the dynamics of on-shell pions (cf. fig. 1). However, the uncertainty of missing one photon due to the limited acceptance of the photon detector or possible background from non-resonance production of $\pi^0\gamma$ might create serious problems for an unambiguous identification of the ω decay products.

For the kinematical conditions of the spectrometer ANKE at the proton accelerator COSY (Jülich) the ω-meson can be produced only close to threshold and therefore will have small transverse momenta. This provides the possibility to separate a signal from the ω decay from an uncorrelated $\pi^0\gamma$ pair using back-to-back correlations in transverse momentum of the π^0 and γ. Alternatively, one can use the distributions in azimuthal angle between two planes $\phi = \phi_{\pi^0} - \phi_\gamma$, where one plane is formed by the initial proton momentum and the π^0 momentum ($\mathbf{p}_0 \wedge \mathbf{p}_{\pi^0}$) and the second one is formed by the initial proton momentum and the γ momentum ($\mathbf{p}_0 \wedge \mathbf{p}_\gamma$). We have demonstrated that the distribution in this azimuthal angle provides quite selective criteria for a separation of the in-medium effect.

We also have investigated, how different kinematical cuts can increase the signal-to-background ratio. The in-medium modifications are found to be most pronounced for the cuts on the total and transverse momentum of the $\pi^0\gamma$ system $P_{\rm tot} \le 0.5$ GeV/c, $P_{\rm t} \le 0.2$ GeV/c and in the azimuthal angle $\phi = \phi_{\pi^0} - \phi_\gamma = 180 \pm 30°$. For example, the ratio $R = \frac{N(M(\pi^0,\gamma)=0.6\text{–}0.75\ \text{GeV})}{N(M(\pi^0,\gamma)\ge 0.75\ \text{GeV})}$, calculated for Pb (C) at $T_p = 2.4$ GeV without cuts, changes from 0.029 (0.008) —when medium effects are absent— to 0.128 (0.059) when both medium effects —collisional broadening and mass shift— are included. The calculations with cuts give the ratio $R = 0.033$ (0.020) without medium effects and 0.401 (0.183) with collisional broadening $\Delta\Gamma \neq 0$ and mass shift $\Delta M \neq 0$ included. Therefore, the study of in-medium effects for ω-mesons via the $\pi^0\gamma$ decay mode in pA collisions in the near-threshold region appears very promising.

The authors acknowledge many useful discussions with K. Boreskov, A. Dolgolenko and A. Sibirtsev throughout this study. The work has been supported by DFG and RFFI.

References

1. G. Brown, M. Rho, Phys. Rev. Lett. **66**, 2720 (1991).
2. C.M. Shakin, W.-D. Sun, Phys. Rev. C **49**, 1185 (1994).
3. W. Cassing, W. Ehehalt, C.M. Ko, Phys. Lett. B **363**, 35 (1995).
4. F. Klingl, W. Weise, Nucl. Phys. A **606**, 329 (1996); F. Klingl, N. Kaiser, W. Weise, Nucl. Phys. A **624**, 527 (1997).
5. T. Hatsuda, S. Lee, Phys. Rev. C **46**, R34 (1992).
6. M. Asakawa, C.M. Ko, Phys. Rev. C **48**, R526 (1993).
7. L.A. Kondratyuk, M. Krivoruchenko, N. Bianchi, E. De Sanctis, V. Muccifora, Nucl. Phys. A **579**, 453 (1994).
8. K.G. Boreskov, J. Koch, L.A. Kondratyuk, M.I. Krivoruchenko, Phys. At. Nucl. **59**, 1908 (1996).
9. B. Friman, Acta Phys. Pol. B **29**, 3195 (1998).
10. F. Klingl, T. Waas, W. Weise, Nucl. Phys. A **650**, 299 (1999).
11. W. Cassing, E.L. Bratkovskaya, Phys. Rep. **308**, 65 (1999).
12. W. Cassing, Ye.S. Golubeva, A.S. Iljinov, L.A. Kondratyuk, Phys. Lett. B **396**, 26 (1997); Ye. Golubeva, L.A. Kondratyuk, W. Cassing, Nucl. Phys. A **625**, 832 (1997).
13. W. Schön, H. Bokemeyer, W. Koenig, V. Metag, Acta Phys. Pol. B **27**, 2959 (1996).
14. Ye.S. Golubeva, A.S. Iljinov, L.A. Kondratyuk, Yad. Phys. **59**, 1891 (1996); Phys. At. Nucl. **59**, 1894 (1996).
15. A. Sibirtsev, V. Hejny, H. Ströher, W. Cassing, Phys. Lett. B **483**, 405 (2000).
16. T. Ericson, W. Weise, *Pions in Nuclei* (Clarendon Press, Oxford, 1988).
17. A. Sibirtsev, Nucl. Phys. A **604**, 455 (1996); A. Sibirtsev, W. Cassing, U. Mosel, Z. Phys. A **358**, 357 (1997).
18. Ye.S. Golubeva, A.S. Iljinov, I.A. Pshenichnov, Nucl. Phys. A **562**, 389 (1993).
19. W. Cassing, S. Juchem, Nucl. Phys. A **665**, 377 (2000).
20. W. Cassing, S. Juchem, Nucl. Phys. A **672**, 417 (2000).
21. W. Cassing, S. Juchem, Nucl. Phys. A **677**, 445 (2000).
22. Ye.S. Golubeva, A.S. Iljinov, B.V. Krippa, I.A. Pshenichnov, Nucl. Phys. A **537**, 393 (1992).
23. J. Cugnon, P. Deneye, J. Vandermeulen, Phys. Rev. C **41**, 1339 (1990).
24. R. Rapp, G. Chanfray, J. Wambach, Nucl. Phys. A **617**, 472 (1997).
25. B. Friman, H.J. Pirner, Nucl. Phys. A **617**, 496 (1997).
26. V. Eletsky, B.L. Ioffe, Phys. Rev. Lett. **78**, 1010 (1997).
27. L. A. Kondratyuk *et al.*, Phys. Rev. C **58**, 1078 (1998).
28. K. Nakayama *et al.*, Phys. Rev. C **57**, 1580 (1998).